




Electrodeposition of low-cost SnS films with increasing carrier concentration and mobility by aluminum doping and texture adjustment

Zhilin Li^{1,*} , Ying Liu¹, Kai Cao¹, Zhengping Zhang¹, and Feng Wang^{1,*}

¹ State Key Laboratory of Chemical Resource Engineering, Beijing Key Laboratory of Electrochemical Process and Technology for Materials, Beijing University of Chemical Technology, Beijing 100029, People's Republic of China

Received: 20 June 2022

Accepted: 15 October 2022

Published online:

4 November 2022

© The Author(s), under exclusive licence to Springer Science+Business Media, LLC, part of Springer Nature 2022

ABSTRACT

SnS is considered being a promising thermoelectric material because it has the same crystal structure as that of SnSe which has excellent thermoelectric properties. However, the low electronic transmission properties confine its performances. The difficult preparation and poor mechanism property of SnS single crystal also confined its commercial application. In this paper, we successfully doped aluminum into the SnS films by a simple one-step co-deposition method. We obtained compact aluminum-doped SnS films with orthogonal crystal structure, which was caused by the properly controlled composition. The carrier concentration of the aluminum-doped SnS films was successful increased by the increase in Al content. The resistivity was further decreased by the additives in the electrolytes because the additives changed the texture orientation and texture coefficient, which caused the change of carrier mobility. When CTAB was added into the electrolytes, the strong (200) texture formed in the aluminum-doped film which caused a relatively large carrier mobility. The combination of the large carrier mobility and concentration determined the resistivity as small as 91.82 $\Omega\cdot\text{cm}$. The results proved that aluminum doping can effectively increase the carrier concentration of SnS films, and the simultaneous carrier mobility decrease can be compensated by additives. The aluminum doping and additive application pave an effective way to promote the electric transition properties of SnS films which is profitable for its thermoelectric characters. And the simplicity of the co-deposition method of aluminum doping and texture adjustment exhibits a potential of commercial application.

Address correspondence to E-mail: lizl@mail.buct.edu.cn; wangf@mail.buct.edu.cn

1 Introduction

Thermoelectric materials have been successfully applied in thermocouple for over a hundred years. For the huge economic and environment profits, reuse of residual or waste heat and electronic refrigeration through thermoelectric effect have long been noticed by researchers [1]. And it was believed that thermoelectric materials have a huge potential for green energy generation because it can realize direct heat-electricity conversion [2]. But the commercial application of thermoelectric phenomenon in power generation has scarce successful example because of the low efficiency. To promote the power generation, the development of thermoelectric materials with high conversion efficiency is the critical factor.

The most convincing parameter to describe thermoelectric performance of a material is figure of merit value which is defined as [1]

$$ZT = S^2\sigma T/\kappa \quad (1)$$

where S , σ , T and κ represent the Seebeck coefficient, the electrical conductivity, the absolute temperature, and the thermal conductivity, respectively. Within such a value, all abilities of thermoelectric potential generation, electrical conductivity and thermal conductivity are taken into account, so ZT can properly reflect the electric power generation efficiency of a material.

SnSe was well noticed recently since it reached the largest ZT value of 2.6 along its b -axis [3–5]. The large ZT of SnSe mainly was caused by its unique layered structure and distortion based on NaCl crystal structure which determines its very small thermal conductivity along b -axis and large conductivity and Seebeck coefficient [3, 6]. In order to increase the ZT of SnSe at different temperatures, many theoretical and experiment attempts were done. One way was change the band gap of SnSe by doping, such as the doping of Pb [1, 7], Te [8]. Another way was changing the phonon transports through the crystal structure change by doping, such as the doping of Cl [2], Br [9]. However, Se is scarce in resource and the toxicity of SeSn may cause water pollution. Furthermore, most observed excellent thermoelectric performance of SeSn appeared in single crystal because it can keep perfect [010] orientation. But single crystal SnSe is difficult to prepare and very brittle, which are disadvantageous for both processing and application.

Therefore, the commercial application of SnSe still has a long way to go.

SnS can be considered as a good substitutional material for SnSe. The reason is that SnS has the same crystal structure as that of SnSe, so it can be expected to have similar thermoelectric properties. Furthermore, SnS is inexpensive, abundant in resource and nontoxic. However, the conductivity of SnS is low for thermoelectric application. One of the reasons is that the band gap of SnS is about 1.3 ~ 1.5 eV, and its carrier concentration is only 10^{15} cm^{-3} at 300 K [10], which is lower than that of most traditional thermoelectric materials [11]. As stated in the literature [12, 13], the carrier concentration between 10^{19} and 10^{21} cm^{-3} is required for high ZT , so the carrier concentration of SnS has to be increased [14–16]. The band gap of the intrinsic semiconductor can be narrowed by the donor or acceptor level provided by doping atoms [17, 18], so doping is an effective path to change band gap and increase carrier concentration. The number of carriers of SnS can be effectively increased through the substitution of Sn or Se atom with doping elements [19]. Many doping elements for SnS, such as Se [20], Cu [21], Na [22], Al [23, 24] and Ag [25–27], were reported to change its transformation characters and thermoelectric properties.

Polycrystal is superior to single crystal in view of both the cost and technique simplicity of preparation. Polycrystal thermoelectric films were prepared with various methods, such as thermal evaporation [28], sol-gel process [29], chemical vapor deposition [30], physical vapor deposition [31] and magnetron sputtering [32]. Electrodeposition is well noticed for its simple process and equipment requirement, low cost and commercial convenience [33]. However, the grain boundary of the deposited polycrystal will cause extra carrier scattering which will decrease the carrier mobility. The advantage of easy carrier movement in special orientation, such as the [010] orientation, of single crystal will lose through electrodeposition because of the random orientations in the polycrystal. In order to keep the advantage, special deposition technique should be adopted to obtain certain preferential orientation. So the texture control of the doping SnS is a precondition of the application of its electrodeposition with high carrier mobility.

In this paper, we attempted the electrodeposition of aluminum-doped SnS and adjust the texture of the films by different additives, in order to promote the carrier concentration and their mobility

simultaneously. Different deposition strategies were attempted to cope with the big reduction potential difference between Al (− 1.66 V, *vs.* RHE) and Sn (− 0.1377 V, *vs.* RHE), in order to fulfill their co-deposition.

2 Experiment methods

2.1 Preparation of the films

We used a three-electrode system to prepare the aluminum-doped SnS thin films. The reference electrode, counter electrode and working electrode were saturated calomel electrode (SCE), Pt plate and indium tin oxide (ITO) substrate with a deposition area of $2 \times 2 \text{ cm}^2$, respectively. Before the electrodeposition, we cleaned the working electrodes with acetone, ethanol and deionized water in turn for 20 min.

The electrolytic bath for SnS film was consisted of 2 mM SnCl_2 , 10 mM $\text{Na}_2\text{S}_2\text{O}_3$ and 6 mM $\text{K}_4\text{O}_2\text{P}_7$. In order to adjust the texture of the films, we added CTAB and urea with the concentration of 10 mg/L into the electrolyte, respectively.

For the aluminum doping SnS thin films, we added different amount of 0.1 M AlCl_3 solution into the electrolyte to obtain the final Al^{3+} concentration of 0 mM, 0.25 mM, 0.50 mM, 0.75 mM and 1.00 mM, respectively. We added dilute sulfuric acid into the electrolyte to adjust the pH to 3.0. The electrodeposition was performed under the potential of −1.1 V (*vs.* SCE) at 50°C for 40 min. We also added CTAB and urea with the concentration of 10 mg/L into the electrolyte to adjust the texture. After the electrodeposition, we placed the obtained thin films into a tube furnace to anneal them at 350°C for 0.5 h with the protection of argon flow.

2.2 Characterization of the films

The crystal structure and texture of the thin films were tested by XRD (RINT 2200 V/PC, Rigaku) with Cu $K\alpha$ radiation at 40 kV, 30 mA and a scan speed of 4°/min. The microscopic morphology and particle homogeneity of the thin films were characterized by SEM (JEOL FE-JSM-6701F, Japan). The acceleration voltage was 5 kV, WD was 8 mm, and the beam strength was 9 μA . The chemical composition of the films was analyzed with an energy-dispersive X-ray

spectroscopy (EDX, Oxford INCA-Penta-FET-X3, England) equipped on the SEM equipment. The test parameters of the EDX were the accelerated voltage of 15 kV and the beam strength of 11 μA . Transmission spectra were recorded with an UV–Vis spectrophotometer (ShimadzuUV-2450, Japan). The band gap E_g of the films was calculated with Eq. (2) according to the transmission test results [34].

$$(\alpha h\nu)^2 = A(h\nu - E_g) \quad (2)$$

Electronic properties such as carrier type, concentration, mobility and the resistivity of the thin films were measured with a Hall effect measurement system (Phys. Tech. RH2030). The measurements were taken along the surface of the films with $1 \times 1 \text{ cm}^2$ test area and 0.5 T magnetic intensity. Before the measurement, the films were peeled off the ITO substrates with marble glue in order to eliminate the interference caused by the substrate.

3 Results and discussion

3.1 Morphology, crystal structure and texture of SnS films

Figure 1(a) shows the morphology of the SnS film deposited without additive. It shows that the film was compact which was composed by homogeneous nano-plates. The compact and homogeneous morphology is profitable for the carrier transformation of the film. When CTAB was added during the electrodeposition, the size of the nano-plates decreased slightly, which is shown in Fig. 1(b). However, after the addition of urea during the electrodeposition, the morphology and the nano-plates almost kept the state of the SnS film without additive [Fig. 1(c)]. Therefore, we can conclude that the additives influence little on the morphology of the films.

The XRD spectra of the films deposited with and without additives are shown in Fig. 2. It shows that all the positions of the peaks match well with the characteristic peak of SnS according to JCPDS 39-0354, except the peaks caused by the ITO substrate. So all the films were SnS with the orthogonal crystal structure, and the additives did not change the crystal structure. However, the relative intensity of the peaks changed much by the additives, which were quite different from those in JCPDS 39-0354. In other words, the additives changed the texture of the

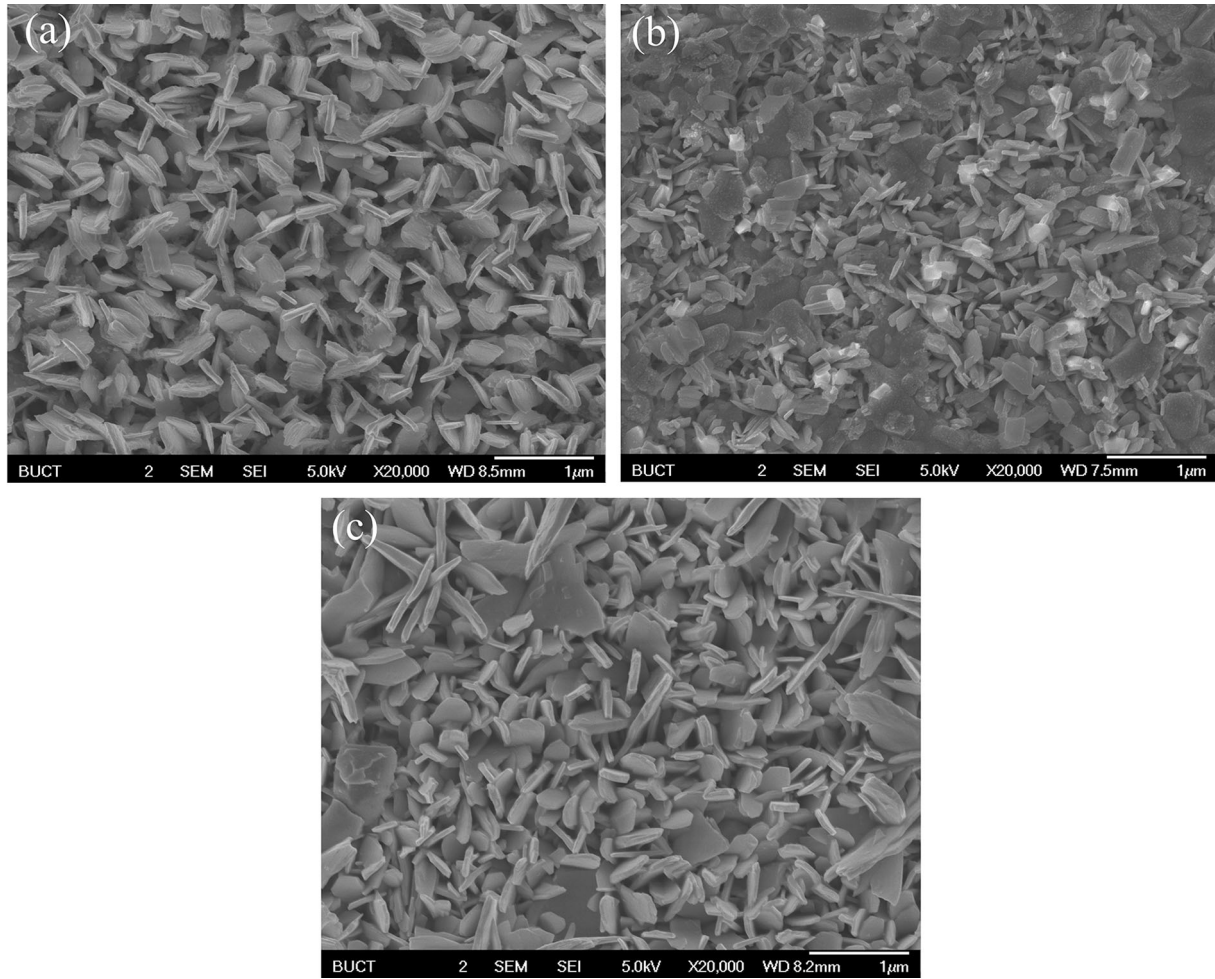


Fig. 1 SEM images of the SnS films: **a** SnS deposited without additive; **b** SnS deposited with CTAB; **c** SnS deposited with urea

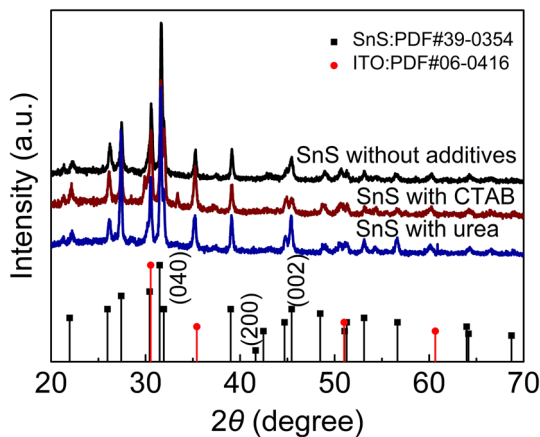


Fig. 2 XRD spectra of the films deposited with and without additives

films. In order to analyze the texture change, we calculated the texture coefficients T_{hkl} of the SnS films with formula (3) [35] based on the XRD test results.

$$T_{hkl} = \frac{I_{hkl}}{I_{hkl}^0} \frac{1}{\frac{1}{n} \sum_{i=1}^n \frac{I_{HKL}}{I_{HKL}^0}} \quad (3)$$

where I_{hkl} represents the tested relative strength of the considering crystal plane (hkl) and I_{hkl}^0 represents the standard relative strength of the diffraction peak of the same crystal plane; I_{HKL} represents the tested relative strength of any crystal plane (HKL) and I_{HKL}^0 represents the standard relative strength of the diffraction peak of the same crystal plane; and n represents the total number of XRD peaks caused by the deposited films. In our case, the value of n is 12, which is the total number of the peaks caused by the diffraction of (110), (120), (021), (111), (040), (131), (200), (141), (002), (151), (122), (042) of orthogonal SnS, respectively.

The calculation results of the texture coefficients of (200), (040) and (002) of the SnS films are shown in

Table 1 Texture coefficients of the SnS films

Additive	T_{200}	T_{040}	T_{002}	Strongest texture
-	1.00	1.67	1.00	(040)
CTAB	2.32	2.14	0.35	(200)
Urea	1.77	2.73	0.67	(040)

Table 1. After the addition of CTAB, the strongest texture orientation changed to (200) crystal plane from (040). Although the addition of urea did not change the strongest texture orientation, it changed the texture coefficient very much. The texture coefficient of the strongest orientation T_{040} changed from 1.67 to 2.73 by the addition of urea. So both the texture orientation and its strength of the SnS films can be effectively adjusted by additives; such change of preferential orientation might cause the change of carrier mobility of the SnS films.

3.2 Aluminum-doped SnS films

Different amount of Al^{3+} was added into the electrolyte to prepare the aluminum-doped SnS films. The compositions of aluminum-doped SnS films were tested by EDX and the results are shown in Table 2. The aluminum content of the films increased with the increase of the Al^{3+} content in the electrolytes, so the aluminum doping amount can be effectively controlled by the adjustment of the Al^{3+} content. The atomic ratio of (Al + Sn):S was successfully controlled between 1:0.90 and 1:0.98, which is quite close to the stoichiometry of SnS. Such an atomic ratio is profitable for the aluminum-doped films to sustain the orthogonal crystal structure of SnS.

Figure 3 shows the SEM images of the aluminum-doped SnS films with different Al content. The aluminum-doped SnS films were still compact and homogenous, but the morphology of the aluminum-doped SnS films changed slightly compared with that

of SnS films. Here, the aluminum-doped SnS films were composed by tiny bars instead of the nanoplates in SnS films.

Figure 4 shows the XRD test results and texture coefficients of aluminum-doped SnS films with different Al content. It can be seen from Fig. 4(a) that all the films still kept the orthogonal crystal structure of SnS, which is in accordance with the atomic ratio of (Al + Sn): S which was close to the stoichiometry of SnS. However, the texture orientations and their strengths were obviously influenced by the aluminum doping. The strongest texture changed from (040) to (200) with the increase in Al content [Fig. 4(b)]. When the Al content reached 1.44-at%, the texture coefficient of (200) crystal plane reached as high as 2.98, which is a very large increase compared with that of 1.00 of pure SnS film (Table 1).

The change of composition and structure of aluminum-doped films caused the corresponding property changes, which is reflected by Fig. 5. With the increase in Al content, the carrier concentration n increased much from $4.26 \times 10^{15} \text{ cm}^{-3}$ to $60.75 \times 10^{15} \text{ cm}^{-3}$. Meanwhile, the carrier mobility μ decreased with the increase in Al content, which could be attributed to the mutual hindrance of the carriers when their concentration was high. Although the carrier mobility decreased, the resistivity ρ decreased after the aluminum doping because of the large carrier concentration increase. Of course the carrier concentration increase could be attributed to the effect of aluminum doping. The reason could be analyzed from Fig. 5(d). After the aluminum doping, the band gap E_g changed from 1.31 eV to 1.21 eV, which is quite close to the reported value [36]. In the aluminum-doped films, Al^{3+} ions should occupy the position of Sn^{2+} cations as donor because Al can contribute 3 electrons. Therefore, Al^{3+} ions provided a donor level below the conduction band resulting in a decrease in the band gap E_g . So more electrons could be excited over the band gap and entered the

Table 2 EDX results of aluminum-doped SnS films deposited in electrolytes with different Al^{3+} content

Al^{3+} content (mM)	Composition (at%)			(Al + Sn):S
	Al	Sn	S	
0.25	0.62 ± 0.22	51.98 ± 1.38	47.40 ± 1.75	1: 0.90
0.50	1.06 ± 0.94	51.13 ± 1.69	47.81 ± 1.13	1: 0.92
0.75	1.38 ± 0.98	50.42 ± 1.97	48.20 ± 4.80	1: 0.92
1.00	1.44 ± 0.23	49.17 ± 0.99	49.39 ± 0.70	1: 0.98

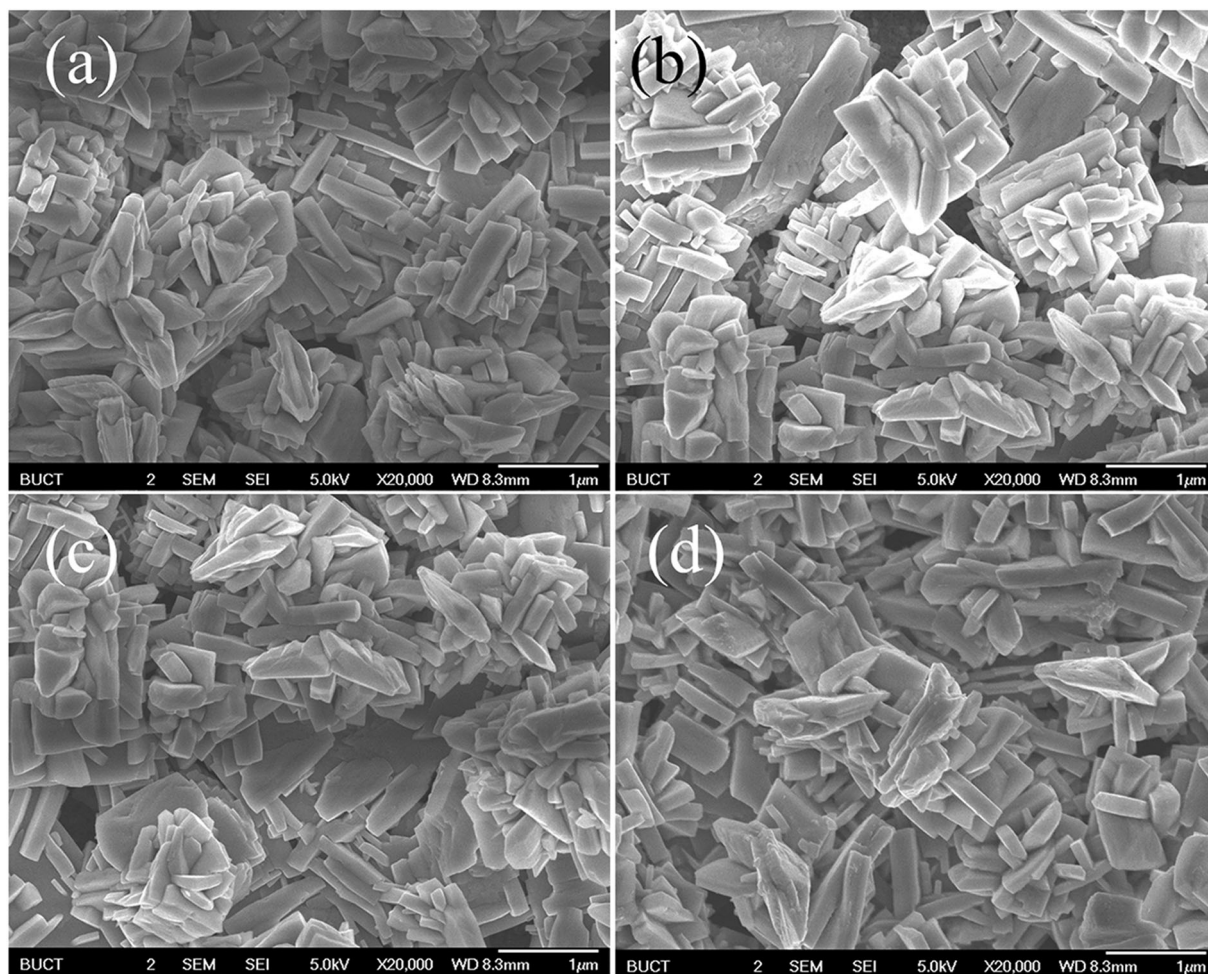


Fig. 3 SEM images of the aluminum-doped SnS films with different Al content: **a** 0.62-at% Al; **b** 1.06-at% Al; **c** 1.38-at% Al; **d** 1.44-at% Al

conduction band to become a carrier [37–39]. By a simple co-deposition method, the aluminum was successfully doped into the SnS films and the Al content was controlled to promote the carrier concentration effectively.

3.3 Aluminum-doped SnS films deposited with additives

It is unsatisfactory that the increase in carrier concentration caused by aluminum doping was accompanied by a carrier mobility decrease. So we attempted to increase the carrier mobility of the aluminum-doped SnS films by the adjustment of texture with additives. The Al^{3+} content of the electrolyte was 1.0 mM, and the content of the additives of CTAB or urea was 10 mg/L. The SEM images of the aluminum-doped SnS films deposited with additives

are shown in Fig. 6. After the addition of the additives, aluminum-doped SnS films were still compact and homogenous, but the morphology changed slightly compared with that without additive. The aluminum-doped SnS films deposited with additives were composed by nano-plates whose thickness was a little larger at the center.

The EDX results of the aluminum-doped SnS films deposited with additives are shown in Table 3. The aluminum content of the films changed after the addition of the additives although the Al^{3+} content in the electrolytes was the same. CTAB increased the aluminum content and urea decreased it. However, the atomic ratio of (Al + Sn):S was still in the range of 1:0.88 to 1:0.97 after the addition, which is quite close to the stoichiometry of SnS. So we can expect that the crystal structure of the aluminum-doped films was still orthogonal at such an atomic ratio.

Fig. 4 XRD spectra and texture coefficients of aluminum-doped SnS films with different Al content: **a** XRD spectra; **b** texture coefficients

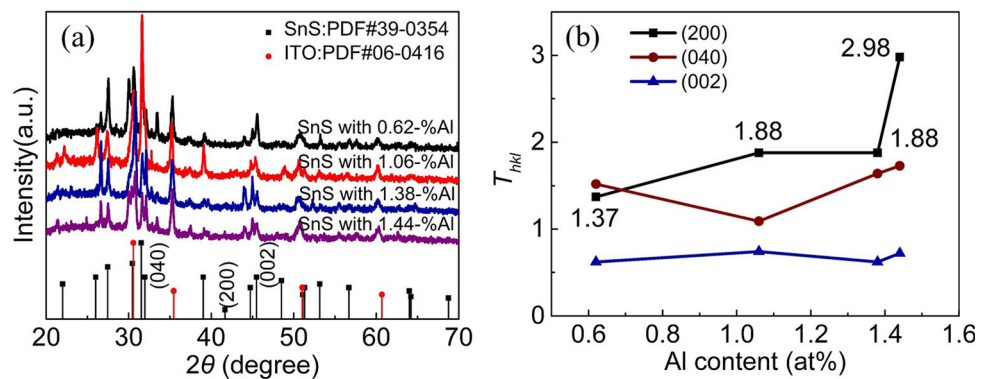


Fig. 5 Hall and band gap test results of aluminum-doped SnS films with different Al content: **a** carrier concentration; **b** carrier mobility; **c** electric resistivity; and **d** band gaps of SnS and aluminum-doped film with 1.44-at % Al

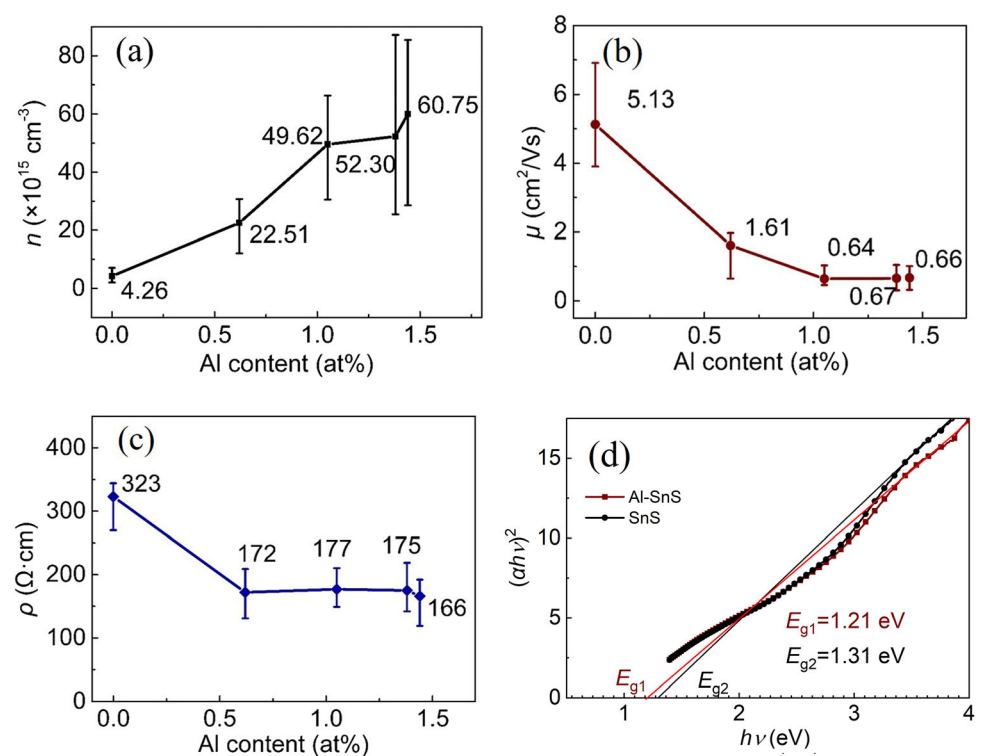


Figure 7 shows the XRD spectra of the aluminum-doped SnS films deposited with additives. It can be seen that all the aluminum-doped SnS films still kept the orthogonal crystal structure, which is in accordance with the atomic ratio of (Al + Sn):S. The texture coefficients of the aluminum-doped SnS films deposited with additives were calculated according to the results in Fig. 7, and the calculation results are listed in Table 3. Comparing the texture characters of the aluminum-doped SnS films deposited with additives with those without additive [Fig. 4(b)] and those without aluminum doping (Table 1), it can be found that the orientations and strengths of the aluminum-doped SnS films were obviously influenced

by the additives. For pure SnS films, CTAB caused the strongest texture orientation change from (040) crystal plane to (200). Urea did not change the strongest texture orientation, but it changed the texture coefficient obviously. For aluminum-doped SnS films, CTAB and urea had the same behavior, but they changed the texture coefficient of the strongest texture much larger. The T_{200} change of the pure SnS film was $2.32-1.00 = 1.32$ by CTAB, but that of the aluminum-doped SnS film was $4.53-2.98 = 1.55$. The T_{040} change of the pure SnS film was $2.73-1.67 = 1.06$ by urea, but that of the aluminum-doped SnS film was $5.76-1.88 = 3.88$. Therefore, the additives had larger effects on textures of aluminum-doped SnS

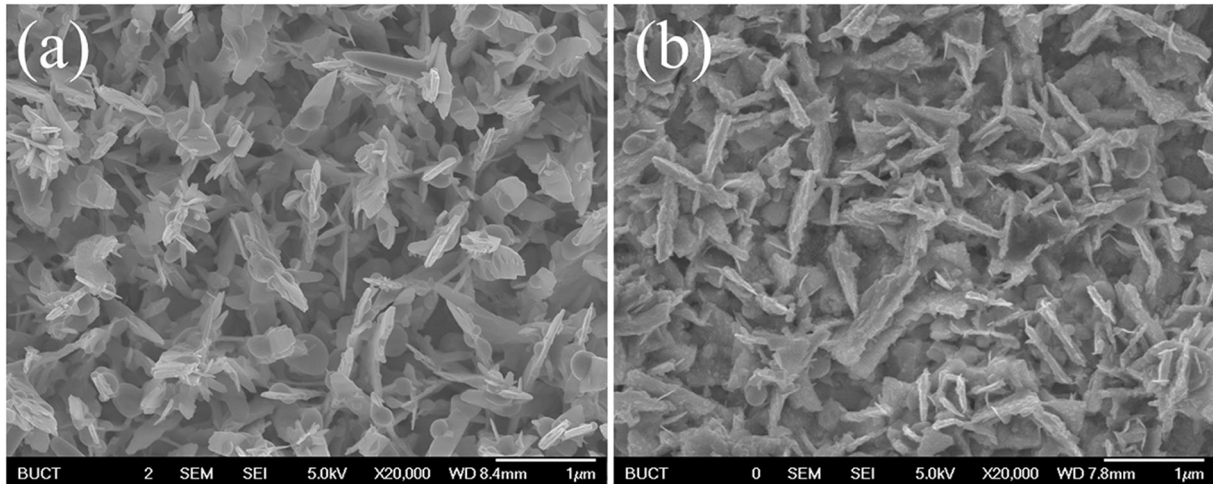


Fig. 6 SEM images of the aluminum-doped SnS films deposited with additives: **a** with CTAB; **b** with urea

Table 3 EDX results and texture coefficients of aluminum-doped SnS films deposited with additives

Additives	Composition (%)			Atomic ratio (Sn + Al):S	T_{200}	T_{040}	Strongest texture
	Al	Sn	S				
-	1.44 ± 0.23	49.17 ± 0.99	49.39 ± 0.70	1:0.98	2.98	1.88	(200)
CTAB	1.54 ± 0.84	48.94 ± 1.18	49.43 ± 1.95	1:0.97	4.53	0.81	(200)
urea	1.32 ± 1.04	51.84 ± 0.87	46.84 ± 0.85	1:0.88	0.22	5.76	(040)

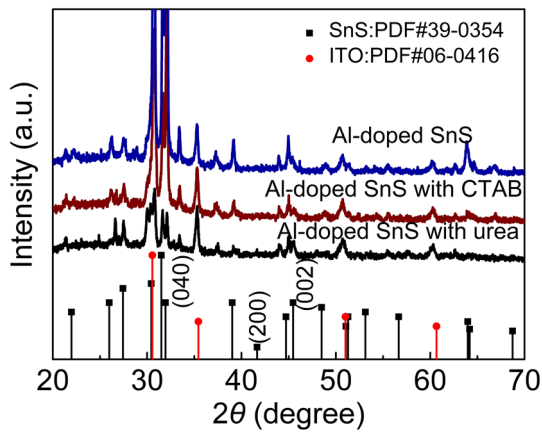


Fig. 7 XRD spectra of the aluminum-doped SnS films with different additives

films. The addition of CTAB is a more effective method to obtain strong texture of *a*-axis, and urea is a more effective method to obtain strong texture of *b*-axis. Therefore, we could adjust the texture of aluminum-doped SnS films more effectively with additives. The stronger textures of the aluminum-doped thin films may bring improved electrical properties.

Such conjecture is confirmed by the electrical property test results in Table 4. The carrier concentration and mobility of the pure SnS film deposited without additives was $4.26 \times 10^{15} \text{ cm}^{-3}$ and $5.13 \text{ cm}^2/\text{V}\cdot\text{s}$, respectively. When pure SnS film deposited with urea, the carrier concentration increased to $12.69 \times 10^{15} \text{ cm}^{-3}$, but the carrier mobility decreased to $0.77 \text{ cm}^2/\text{V}\cdot\text{s}$, so the resistivity increased from $323.22 \text{ }\Omega\cdot\text{cm}$ to $700.48 \text{ }\Omega\cdot\text{cm}$. Such a large resistivity increase in resistivity is unwelcome. However, when pure SnS film deposited with CTAB, the carrier concentration increased to $6.12 \times 10^{15} \text{ cm}^{-3}$, and the carrier mobility increased to $7.44 \text{ cm}^2/\text{V}\cdot\text{s}$ simultaneously, which caused an encouraging resistivity decrease to $174.21 \text{ }\Omega\cdot\text{cm}$. Such decrease came from the texture change from (040) to (200), which obviously increased the carrier mobility and did not decrease the carrier concentration.

After the aluminum doping, the carrier concentration increased noticeably, which caused the resistivity decrease for all aluminum-doped films. The carrier concentration increased to $60.76 \times 10^{15} \text{ cm}^{-3}$, which was a large increase. But the resistivity did not

Table 4 Electrical performance of pure and Al-doped SnS films with different textures

Doping state	Additive	Strongest texture	T_{hkl}	n ($\times 10^{15} \text{ cm}^{-3}$)	μ ($\text{cm}^2/\text{V}\cdot\text{s}$)	ρ ($\Omega\cdot\text{cm}$)
pure	–	(040)	1.67	4.26	5.13	323.22
pure	CTAB	(200)	2.32	6.12	7.44	174.21
pure	urea	(040)	2.73	12.69	0.77	700.48
aluminum-doped	–	(200)	2.89	60.76	0.67	166.04
aluminum-doped	CTAB	(200)	4.54	74.16	1.05	91.82
aluminum-doped	urea	(040)	5.76	129.45	0.51	104.17

decrease to the same extent because the carrier mobility decreased much simultaneously. The largest carrier concentration of $129.45 \times 10^{15} \text{ cm}^{-3}$ occurred on the SnS film deposited with urea, but the carrier mobility decreased too much simultaneously, so the resistivity of the film was not the smallest. When the aluminum-doped SnS film was deposited with CTAB, the carrier concentration reached $74.16 \times 10^{15} \text{ cm}^{-3}$, and the carrier mobility decreased smallest for the aluminum-doped SnS films because the strongest texture changed to (200) now. By the aluminum doping and texture adjustment with additives, the resistivity of the aluminum-doped film decreased to $91.82 \Omega\cdot\text{cm}$, which is delightful because it is smaller than the 1/3 of the original value of the pure SnS films.

The ZT value of our Al-doped SnS thin films can be analyzed as the follows. The largest carrier concentration of $129.45 \times 10^{15} \text{ cm}^{-3}$ reached the same level of that of Si nano-wire of $1 \times 10^{17} \text{ cm}^{-3}$ [40]. The resistivity of the same film of $104.17 \Omega\cdot\text{cm}$ is a little larger than that of the Si nano-wire because of the smaller carrier mobility. However, the (040) texture of the film should have the very small thermal conductivity along b -axis and large Seebeck coefficient, which is determined by its unique layered structure and distortion based on NaCl crystal structure [3, 6]. Furthermore, ref. [40] stated that the thermal conductivity of doped Si nano-wires will be reduced when its diameter is thinner than 300 nm but more than 110 nm, because its phonon mean free path is ~ 300 nm, while its electron mean free path is ~ 110 nm. The thickness of the nano-plates of our Al-doped films is just in this range (Fig. 6). Suppose the films had the similar phonon mean free path and electron mean free path as those of Si nano-wire, their nano-structure is also profitable for the decrease of thermal conductivity. All this factors are quite beneficial to increase ZT .

Our results proved that aluminum doping can effectively increase the carrier concentration of SnS films, but it decreased the carrier mobility simultaneously. The carrier mobility of aluminum-doped SnS films could be increased by texture adjustment by additives. Such combination of doping and texture reached a highest conductivity of SnS films by the increase in carrier concentration and mobility simultaneously. The aluminum doping and additive application pave an effective way to promote the electric transition properties of SnS films which is profitable for its thermoelectric characters. And the simplicity of the co-deposition method of aluminum doping and texture adjustment by additives exhibits a potential of commercial application.

4 Conclusions

SnS films and aluminum-doped SnS films were prepared by potentiostatic electrodeposition. The SnS films were compact which was composed by homogeneous nano-plates with the expected orthogonal crystal structure. The (200) and (040) texture with large texture coefficients were successfully obtained by adding CTAB and urea during the deposition, respectively. The smallest resistivity was obtained in the SnS film deposited with CTAB, which was determined by the large carrier concentration and the largest carrier mobility caused by the (200) texture.

By a simple co-deposition method, the aluminum was successfully doped into the SnS films and the Al content was controlled by the Al^{3+} content in the electrolytes. Aluminum-doped SnS films were also compact with the expected orthogonal crystal structure because of the successfully controlled composition which was close to the stoichiometry of SnS. The carrier concentration of the aluminum-doped SnS films increased with the increase in its Al content because the doped Al decreased the band gap E_g . The

resistivity of the aluminum-doped SnS films was further decreased by the additives in the electrolytes during the electrodeposition. The reason is that the additives changed the texture orientation and texture coefficient, which caused the change of carrier mobility. When CTAB was added into the electrolytes during the electrodeposition, the strong (200) texture formed in the aluminum-doped film with the large texture coefficient of 4.54 which caused a relatively large carrier mobility of $1.05 \text{ cm}^2/\text{V}\cdot\text{s}$. The combination of the large carrier mobility and the large carrier concentration of $74.16 \times 10^{15} \text{ cm}^{-3}$ caused by the aluminum doping determined the resistivity as small as $91.82 \text{ }\Omega\cdot\text{cm}$, which is smaller than the 1/3 of the original value of the pure SnS films.

Our results proved that aluminum doping can effectively increase the carrier concentration of SnS films, and the carrier mobility decrease can be compensated by additives. The aluminum doping and additive application pave an effective way to promote the electric transition properties of SnS films which is profitable for its thermoelectric characters. And the simplicity of the co-deposition method of aluminum doping and texture adjustment exhibits a potential of commercial application.

Author contributions

All authors contributed to the study conception and design. Material preparation and data collection were performed by YL, and data analysis was performed by ZL and YL. The first draft of the manuscript was written by YL, and all authors commented on previous versions of the manuscript. All authors read and approved the final manuscript.

Funding

This work was supported by the National Natural Science Foundation of China (Grant No. 51472020).

Data availability

All data generated or analyzed during this study are included in this published article.

Declarations

Competing interests The authors declare that there is no competing interest to disclose that is directly or indirectly related to the work submitted for publication.

Research involving human and animal rights The authors have no relevant financial or non-financial interests to disclose. This work involved no human participants and animals and had no informed consent.

References

1. B. Qin, D. Wang, X. Liu, Y. Qin, J.F. Dong, J. Luo, J.W. Li, W. Liu, G. Tan, X. Tang, J.F. Li, J. He, L.D. Zhao, *Science* **373**, 556 (2021)
2. L. Su, D. Wang, S. Wang, B. Qin, Y. Wang, Y. Qin, Y. Jin, C. Chang, L.D. Zhao, *Science* **375**, 1385 (2022)
3. L.D. Zhao, S.H. Lo, Y. Zhang, H. Sun, G. Tan, C. Uher, C. Wolverton, V.P. Dravid, M.G. Kanatzidis, *Nature* **508**, 373 (2014)
4. L.D. Zhao, G. Tan, S. Hao, J. He, Y. Pei, H. Chi, H. Wang, S. Gong, H. Xu, V.P. Dravid, C. Uher, G.J. Snyder, C. Wolverton, M.G. Kanatzidis, *Science* **351**, 141 (2016)
5. Y. Xiao, L.D. Zhao, *Science* **367**, 1196 (2020)
6. Y. Xiao, C. Chang, Y. Pei, D. Wu, K. Peng, X. Zhou, S. Gong, J. He, Y. Zhang, Z. Zeng, L.D. Zhao, *Phys. Rev. B* **94**, 125203 (2016)
7. C. Chang, D. Wang, D. He, W. He, F. Zhu, G. Wang, J. He, L.D. Zhao, *Adv. Energy Mater.* **9**, 1901334 (2019)
8. B. Qin, D. Wang, W. He, Y. Zhang, H. Wu, S.J. Pennycook, L.D. Zhao, *J. Am. Chem. Soc.* **141**, 1141 (2019)
9. C. Chang, M. Wu, D. He, Y. Pei, C.F. Wu, X. Wu, H. Yu, F. Zhu, K. Wang, Y. Chen, L. Huang, J.F. Li, J. He, L.D. Zhao, *Science* **360**, 778 (2018)
10. T. Gotoh, *Phys. Status Solidi A*. **213**, 1869 (2016)
11. R. Guo, X. Wang, Y. Kuang, B. Huang, *Phys. Rev. B* **92**, 1 (2015)
12. T.M. Tritt, *Science* **283**, 804 (1999)
13. J. Yang, L. Xi, W. Qiu, L. Wu, X. Shi, L. Chen, J. Yang, W. Zhang, C. Uher, D.J. Singh, *NPJ. Comput. Mater.* **2**, 1 (2016)
14. B.Z. Sun, Z. Ma, C. He, K. Wu, *RSC Adv.* **5**, 56382 (2015)
15. Q. Tan, C.F. Wu, W. Sun, J.F. Li, *RSC Adv.* **6**, 43985 (2016)
16. H.S. Kim, Z.M. Gibbs, Y. Tang, H. Wang, G.J. Snyder, *APL Mater.* **3**, 041506 (2015)
17. N.K. Singh, S. Bathula, B. Gahtori, K. Tyagi, D. Haranath, A. Dhar, *J. Alloys Comp.* **668**, 152 (2016)

18. E.K. Chere, Q. Zhang, K. Dahal, F. Cao, J. Mao, Z. Ren, J. Mater. Chem. A. **4**, 1848 (2016)
19. D.M. Unuchak, K. Bente, V.A. Ivanov, V.F. Gremenok, Cryst. Res. Technol. **45**, 1113 (2010)
20. W. He, D. Wang, H. Wu, Y. Xiao, Y. Zhang, D. He, Y. Feng, Y.J. Hao, J.F. Dong, R. Chetty, L. Hao, D. Chen, J. Qin, Q. Yang, X. Li, J.M. Song, Y. Zhu, W. Xu, C. Niu, X. Li, G. Wang, C. Liu, M. Ohta, S.J. Pennycook, J. He, J.F. Li, L.D. Zhao, Science **365**, 1418 (2019)
21. Y. Goto, F. Naito, R. Sato, K. Yoshiyasu, T. Itoh, Y. Kamihara, M. Matoba, Inorg. Chem. **52**, 9861 (2013)
22. V. Steinmann, R.E. Brandt, R. Chakraborty, R. Jaramillo, M. Young, B.K. Ofori-Okai, C. Yang, A. Polizzotti, K.A. Nelson, R.G. Gordon, T. Buonassisi, APL Mater. **4**, 026103 (2016)
23. M.A. Almessiere, A.L. Al-Otaibi, I.B. Assaker, T. Ghrib, R. Chtourou, Mater. Sci. Semicond. Proc. **40**, 267 (2015)
24. Y. Yang, S. Cheng, J. Semico. **29**, 2322 (2008)
25. O. Falkenbach, J. Tinz, A.S. Schulze, E. Mueller, S. Schlecht, Phys. Status Solidi A. **213**, 699 (2016)
26. C. Bera, S. Jacob, I. Opahle, N.S. Gunda, R. Chmielowski, G. Dennler, G.K. Madsen, Phys. Chem. Chem. Phys. **16**, 19894 (2014)
27. S. Bhattacharya, N.S. Gunda, R. Stern, S. Jacobs, R. Chmielowski, G. Dennler, G.K. Madsen, Phys. Chem. Chem. Phys. **17**, 9161 (2015)
28. Y. Kawano, J. Chantana, T. Minemoto, Curr. Appl. Phys. **15**, 897 (2015)
29. J. Sun, Y. Huang, S. Nie, Z. Chen, J. Xu, L. Zhao, W. Zhou, Q. Wang, H. Gong, Mater. Lett. **178**, 231 (2016)
30. H. Zhang, Y. Balaji, A.N. Mehta, M. Heyns, M. Caymax, I. Radu, W. Vandervorst, A. Delabie, J. Mater. Chem. C **6**, 6172 (2018)
31. J. Xia, X.Z. Li, X. Huang, N. Mao, D.D. Zhu, L. Wang, H. Xu, X.M. Meng, Nanoscale **8**, 2063 (2016)
32. M. Patel, A. Ray, RSC Adv. **4**, 3934 (2014)
33. B. Ghosh, R. Roy, S. Chowdhury, P. Banerjee, S. Das, Appl. Surf. Sci. **256**, 4328 (2010)
34. H. Kafashan, F.J. Sheini, R.E. Kahrizsangi, R. Yousefi, J. Alloys Comp. **681**, 595 (2016)
35. A.A. Ramadan, A.A. Abd El-Mongy, A.M. El-Shabiny, A.T. Mater, S.H. Mostafa, E.A. El-Sheheedy, H.M. Hashem, Cryst. Res. Technol. **44**, 111 (2009)
36. H. Kafashan, R.E. Kahrizsangi, F.J. Sheini, R. Yousefi, Phys. Status Solidi A **213**, 1302 (2016)
37. C. Wu, L. Shen, H. Yu, Q. Huang, Y.C. Zhang, Mater. Res. Bull. **46**, 1107 (2011)
38. G. Kaur, A. Mitra, K.L. Yadav, Prog. Nat. Sci. Mater. **25**, 12 (2015)
39. C.E. Benouis, M. Benhaliliba, Z. Mouffak, A.A. Garcia, A.T. Silver, M.O. Lopez, R.R. Trujillo, Y.S. Ocak, J. Alloys Compd. **603**, 213 (2014)
40. Y. Li, G. Wang, M.A. Saatlu, M. Procek, H.H. Radamson, Frontiers Mater. **8**, 611078 (2021)

Publisher's Note Springer Nature remains neutral with regard to jurisdictional claims in published maps and institutional affiliations.

Springer Nature or its licensor (e.g. a society or other partner) holds exclusive rights to this article under a publishing agreement with the author(s) or other rightsholder(s); author self-archiving of the accepted manuscript version of this article is solely governed by the terms of such publishing agreement and applicable law.